Monitoring of Self-Healing composites: a non-linear ultrasound approach

Gian-Piero Malfense Fierro[a], Fulvio Pinto[a], Stefania Dello Iacono[b], Alfonso Martone[b], Eugenio Amendola[b], Michele Meo[a1]

[a] University of Bath, Materials Research, Department of Mechanical Engineering, Claverton Down, Bath, UK

[b] National Research Council, Institute for Polymers, Composites and Biomaterials, P.le Enrico Fermi 1, 80055 Portici (NA), Italy

Abstract

Self-healing composites using a thermally mendable polymer based on Diels–Alder reaction were fabricated and subjected to various multiple damage loads. Unlike the traditional destructive methods, this work presents a nonlinear ultrasound technique to evaluate the efficiency of the structural recovery of the proposed self-healing laminate structures. The results were compared to Computer Tomography (CT) and linear ultrasound methods. The laminates were subjected to multiple loading/healing cycles and the extent of damage at each of these stages was evaluated using various NDT/E techniques. The results highlight the benefit and added advantage of the use of a nonlinear based methodology to monitor the structural recovery of self-healing composites.

Keywords: Nonlinear Ultrasound, Phased Array, Self-Healing, Composite, Computer Tomography (CT)

1. Introduction

Over the last twenty years, the advancement of material technology and composite manufacturing techniques has expanded with the number of applications in which carbon fibres reinforced polymers (CFRP) can be employed. CFRP applications range from a very specific highly technological environment (aerospace, Formula 1 and nuclear) to mass market applications (sport equipment, automotive and energy applications). This is due to CFRPs very high specific properties and versatility which make them perfect for utilisation in those applications that require very good mechanical properties and low weight [1].

However, because of their intrinsic layered structure, composite laminates are characterised by weak resistance in the out-of-plane direction, which make them susceptible to damage growth and propagation when subjected to an impact event [2]. Indeed, due to the high stiffness and low strain given by the carbon fibres, composite materials cannot deform plastically, hence low impact in the out-of-plane direction will lead to the formation of barely visible impact damage (BVID) that if not immediately identified could cause critical failure of the entire structure.

Based on these premises, the possibility of recovering the integrity of a damaged composite component constitutes a fundamental breakthrough in the development of advanced composite systems and has attracted the attention of several researchers, leading to the development of a new class of smart systems called self-healing materials [3-5].

From the current literature it is possible to identify three different classes of self-healing materials that can be summarised as intrinsic, extrinsic and shape-memory assisted. Intrinsic or remediable self-healing systems are based on polymers that can repair themselves by exploiting the reversibility of specific reactions such as the Diels-Alder [6, 7] or the presence of thermoreversible functional groups, such as disulphide or ester [8-10]. Extrinsic self-healing materials are systems that incorporate capsules filled with a healing agent, such as diclycopentadiene: when a damage occurs,

[1] Corresponding author: m.meo@bath.ac.uk

the capsules are fractured and the healing agent fills the damaged area and solidifies due to the catalyst particles dispersed into the resin [11, 12]. Vascular self-healing materials are an improvement of capsule-based extrinsic materials inspired by biological systems and are based on the presence of a complex system of micro-channels (similar to blood vessels) incorporated within a polymer matrix that can deliver the reactive fluid in damaged areas in order to mend them [13, 14]. As for the shape-memory assisted self-healing materials, they are based on the inclusion of shape memory materials such as shape memory alloys wires (SMA) [15] or shape memory polymer (SMP) both in form of fibres [16] or "bulk" [17] to partially or fully close cracks. Once activated these materials are able to exert a local contractual force that pulls the crack surfaces closer, healing the damaged material. All these systems have been proved to be very effective for the recovering of the mechanical properties of composite laminates subjected to impact damage under different destructive approaches, however very few works have been focused on the use of non-destructive techniques to monitor the healing process and to measure the recovery of the healed portion of the material.
In particular, apart from Raman Spectroscopy which is probably the most common technique used for this kind of investigation [18, 19], the vast majority of literature in this subject is focused on the use of ultrasonics for the monitoring of healing processes in concrete systems. For instance, In et al [20] have used ultrasonic waves to measure the effectiveness of the healing process in fractured concrete samples. In particular, by analysing diffuse ultrasonic parameters such as effective ultrasonic diffusivity and Arrival Time of Maximum Energy (ATME) it is possible to monitor the self-healing process over time, although the proposed method shows some fluctuations due to partial crack closure. The decrease of the ultrasonic pulse velocity (UPV) was also used to measure the extent of the healing process in cracked concrete samples, as illustrated in the work by Zhong and Yao [21]. In their work they identify a relationship between the extent of a damaged area and the healing effect by correlating the UPV measures with the strength increment after the healing process for both normal and high strength concrete samples.
In a different approach, non-destructive methods were used to assess the effect of the presence of an embedded vascular system in bioinspired self-healing composites, as illustrated in a study conducted by Coppola et al, in which they used acoustic emission to monitor in real-time the behaviour of vascular composite sample subjected to tensile tests [22]. The effectiveness of the healing processes was also monitored using a technique based on time reversal of acoustic waves as demonstrated by Granger et al, who correlated the drift of a signal emitted initially in high performance concrete samples with the presence of damaged areas. By analysing different signals collected during a bending/healing cycle and then time reversed on a sensor positioned near the expected crack path it is possible to observe a decrease in amplitude due to cracking and an increase as a result of the healing process [23].
In this context, this paper is focused on the use of different non-destructive techniques to analyse the effectiveness of the healing process in composite laminates prepared using Diels-Alder epoxy adducts. The methods comprised of CT-Scans and various ultrasound pulse/echo techniques, with the focus on evaluating the potential of a nonlinear ultrasound phased array technique to assess damage recovery. The CT-Scan tests were used as the control to evaluate the performance of the other ultrasound techniques as they provide the highest definition and damage assessment capabilities. Thus, the focus has been on evaluating various ultrasound techniques due to their capability, flexibility and relative cost-effectiveness. The analysis was conducted by following both linear and non-linear approaches, investigating the behaviour of several composite samples subjected to a cycle consisting of multiple end-notch-failure tests followed by healing.

2. Experimental procedure

As previously illustrated, one of the most used chemical approaches to implement healing into polymeric matrices is the use of Diels Alder (D-A) chemistry, hence, this typology of self-healing materials was chosen to test the effectiveness of the different NDT techniques.
The resin used for the manufacturing of the samples is a self-healing epoxy system 2Ph2Epo65, manufactured by Amendola et al [7, 24], which is based on the introduction of diene and a dienophile moieties in the polymer precursors which are used as reversible crosslinkers. The use of furan-

maleimide Diels-Alder moieties allows for the synthesis of epoxy resins with reversible crosslinks capable of multiple healing events upon thermal stimulus. The coexistence of a stable polymeric network and a thermo-reversible one is one of the preferred paths to develop self-healing materials with robust self-healing ability and good mechanical behaviour during healing [25].
In order to evaluate the effectiveness of the healing mechanism, different samples were manufactured and subjected to shear tests over multiple healing processes. Table 1 illustrates the different phases of the experimental procedure including the different NDT techniques, the mechanical tests and the healing processes.

Table 1 - Step-by-step experimental procedure

Step	Test Procedure	Damage State
1	Phased Array Testing 1	Undamaged
2	Water Tank C-Scan 1	Undamaged
3	CT-Scan 1	Undamaged
4	SHEAR TEST 1	Induce Damage 1 (D1)
5	Phased Array Testing 2	D1
6	Water Tank C-Scan 2	D1
7	CT-Scan 2	D1
8	**Healing 1**	D1/Heal 1 (H1)
9	Phased Array Testing 3	D1/H1
10	Water Tank C-Scan 3	D1/H1
11	CT-Scan 3	D1/H1
12	SHEAR TEST 2	Induce Damage 2 (D2)
13	Phased Array Testing 4	D1/H1/D2
14	Water Tank C-Scan 4	D1/H1/D2
15	CT-Scan 4	D1/H1/D2
16	**Healing 2**	D1/H1/D2/ Heal 2 (H2)
17	Phased Array Testing 5	D1/H1/D2/H2
18	Water Tank C-Scan 5	D1/H1/D2/H2
19	CT-Scan 5	D1/H1/D2/H2
20	SHEAR TEST 3	Induce Damage 3 (D3)
21	Phased Array Testing 4	D1/H1/D2/H2/D3
22	Water Tank C-Scan 4	D1/H1/D2/H2/D3
23	CT-Scan 6	D1/H1/D2/H2/D3

The selected healing cycle is a two-step thermal treatment:
- I step: heating 20 min at 120°C, to induce the rD-A reaction, to activate diene and dienophile reacting pairs and increase molecular mobility required to let molecular segments diffuse across the fracture surface;
- II step: annealing 12 hours at 90°C, to promote the direct D-A recombination and restore resin crosslinked structure.

3. Self-Healing Information

Structural formulae of all components used in the preparation of self-healing epoxy 2Ph2Epo65 are described in Figure 1. The suffix -65 refers to the percentage of Diels-Alder epoxy (2Ph2Epo), with respect to the total epoxy used. 2Ph2Epo epoxy precursor is characterized by the presence of two oxirane rings and two Diels Alder adducts.

Its synthesis was already described elsewhere [24]. Diglycidyl ether of bisphenol A (DGEBA) with an Epoxy Equivalent Weight of 185-190 g/eq was kindly supplied by Elantas S.p.A. with commercial name of EC01.

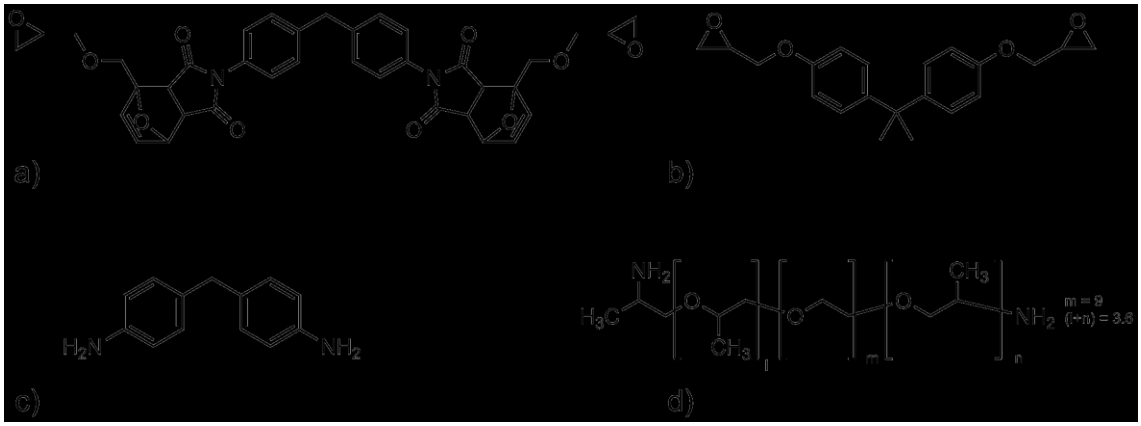

Figure 1 - Main chemical components of the 2Ph2Epo65 compound. a) 2Ph2Epo adduct, b) DGEBA, c) DDM, d) Jeff500 ammine

DDM and Jeff 500 were purchased from Sigma and used without further purification in the stoichiometry ratio of DDM/Jeff500 = 60/40. The flexible amine Jeff500 was added to the formulation in order to limit the glass transition temperature of the completely crosslinked system to the value of about 90°C. In fact, a higher value of Tg would require high curing temperature potentially interfering with the Diels-Alder and rDiels-Alder reactions responsible for self-healing phenomena.Curing was performed at 90°C for 24 hours. The epoxy and amine groups were stoichiometrically balanced before curing.

Mechanical tests carried out on the formulated D-A epoxy showed its ability to recover stiffness after multiple testing cycles (bending failure and thermal healing). The 2Ph2Epo65 epoxy resin showed a progressive decrease of the strength in further cycles while the stiffness is restored (Figure 2). Since the samples were able to recover all their original stiffness, probably further thermal treatment could affect the DGEBA network, modifying the failure mechanism of the sample [7].

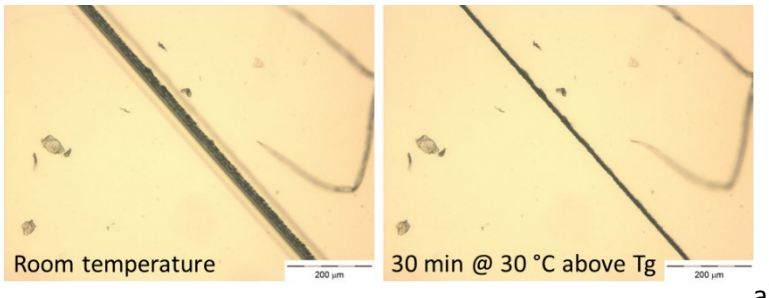

a)

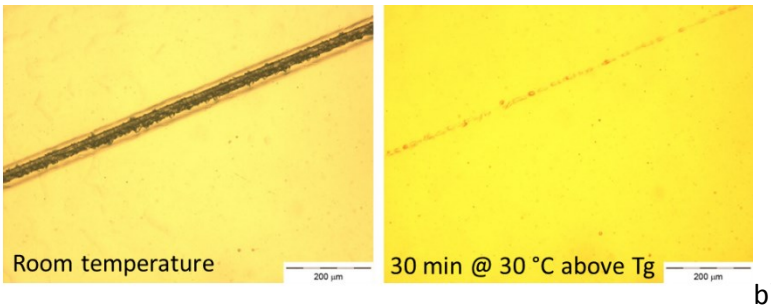

Figure 2 - Difference between the behaviour of a traditional resin system and the remendable 2Ph2Epo65 epoxy when subjected to a damage-heating cycle.

4. Mechanical Testing

Shear tests can be conducted on composite laminates following different experimental approaches, depending on the mode of fracture that needs to be assessed. Due to the layered structure of composite laminates, in this work the effect of the self-healing epoxy resin and its healing capability were investigated under mode II fracture loading by performing End Notch Failure (ENF).
A Composite plate has been manufactured by liquid moulding process under vacuum bag, 12 unidirectional layers were laminated to reach a nominal thickness of 3 mm. A polyimide film (Kapton) was lied down at the mid plane to induce an initial delamination. Table 2 reports geometry of two samples (S1 and S2) cut from the plate. The presence of a Kapton layer in a bending test (End Notched Failure, ENF) leads to the mutual sliding of separated parts promoting a Mode II failure (shear mode) according to ASTM D7905.
ENF tests were carried out by positioning the different samples in an Instron 3369 Universal Testing Machine using a three point bending setup. The crosshead was then lowered with a constant speed of 4 mm/min in order to apply a load on the central portion of the sample and propagate the crack from the edge of the embedded Kapton film towards the loading point through the length of the specimen. Sample dimensions and the parameters of the ENF tests are illustrated in Table 2 and Figure 3.

Table 2 - Geometrical and experimental parameter of the End Notch Failure (ENF) tested samples

Number of Plies	Length	Width	Thickness	Position of the kapton film
12	120 mm	25 mm	3 mm	middle section
Span Length	Crosshead velocit	Initial crack lengt	Load Pin dimensic	Support Pins dimension
100 mm	4 mm/min	40 mm	6 mm	6 mm

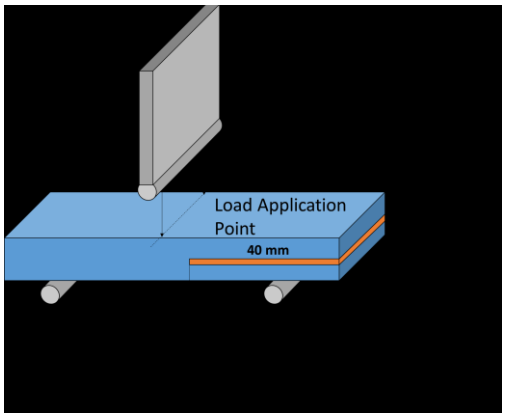

Figure 3 - End Notch Failure (ENF) Test experimental setup

Figure 4 and Figure 5 show the load-extension curves collected for both Sample 1 and Sample 2 during the entire experimental campaign (three loading cycles for each sample).

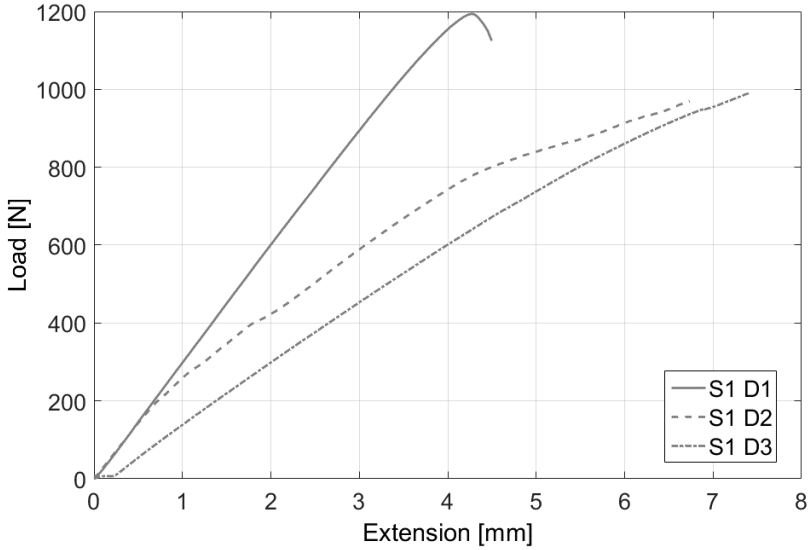

Figure 4 - Load - Displacement curves obtained for the Sample 1 during the entire experimental campaign

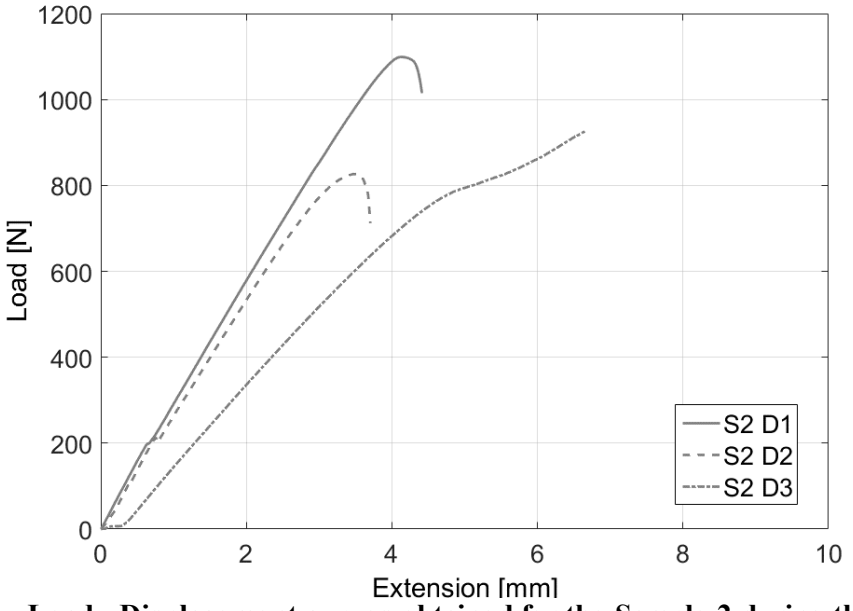

Figure 5 - Load - Displacement curves obtained for the Sample 2 during the entire experimental campaign

Sample 1 and Sample 2 are representative of possible scenarios, a non-complete recovery due to poor compaction pressure during treatment and a proper healing procedure, respectively. Sample 2 recovered its pristine stiffness after the first healing cycle, even if a slight decrease of the critical load is reported in further healing/loading cycles. Sample 1 showed quite different behaviour; the test after first healing cycle showed initially the same stiffness of pristine material, however, there was an abrupt deviation after 200 N. The effect of this "incomplete" healing and a comparison with a completely healed samples over different healing/damage cycles will be analysed in detail in the next paragraphs.

5. Non-destructive testing (NDT) of recovery process

Ultrasound testing can be broken into many different groups and testing methods which vary depending on the various parameters used to evaluate damage/defects. In this piece of work the focus has been to evaluate various methods than focus on the evaluation of pulse/echo responses through the thickness of the tested medium to determine damage. The simplest of these methods is the Water Tank C-Scan, which uses a single element piezoelectric transducer to transmit and capture signal responses and has been already employed by several authors to evaluate crack self-healing performance [26, 27]. The next method used was a traditional ultrasound phased array system, which operates with the same basic principles as the Water Tank C-Scan method, although it relies on an array of piezoelectric transducers where the sequence of firing and capturing determines the accuracy. Traditionally, these two methods rely on evaluating the response signal in the time domain, by evaluating responses captured as peaks at the front and back wall of the testing medium (echoes), with damage being highlighted as a peak between these two surfaces of the structure.
Phased array techniques are arguably leading the field in ultrasonic testing, recent focus has been on the development of nonlinear ultrasound phased array [28, 29]. The primary focus of this work is to evaluate the effectiveness of a nonlinear based ultrasound phased array technique in imaging the recovery process of the testing self-healing structures. In order to evaluate nonlinear behaviour (the production of higher order harmonics), the presence of damage was correlated to higher harmonics.

Nonlinear ultrasound phased array and imaging techniques have been assessed by the following authors [30-34]; Ohara *et al* and Park *et al* have extensively developed, evaluated and improved the detection of open and closed cracks in metallic structures using a subharmonic phased array, while Potter *et al* has developed a nonlinear array based on the traditional total focusing method (TFM). These works have not focused on composite material or healing evaluation using these techniques.

5.1. CT-Scan

Figure 6 below shows the CT-Scan layout for the undamaged (green) and damaged (red) scanned areas. Initially the whole undamaged sample was scanned in order to evaluate whether damage was present in the samples. The red solid line on the sample indicates the end of the Kapton layer (40mm in length). After the first damage cycle the scanned area was reduced in order to increase the CT resolution, undamaged area resolution ~ 90 microns, damaged area resolution ~ 35 microns. CT resolution depends on the size of the area being inspected and the minimum resolution that can be obtained by the system.

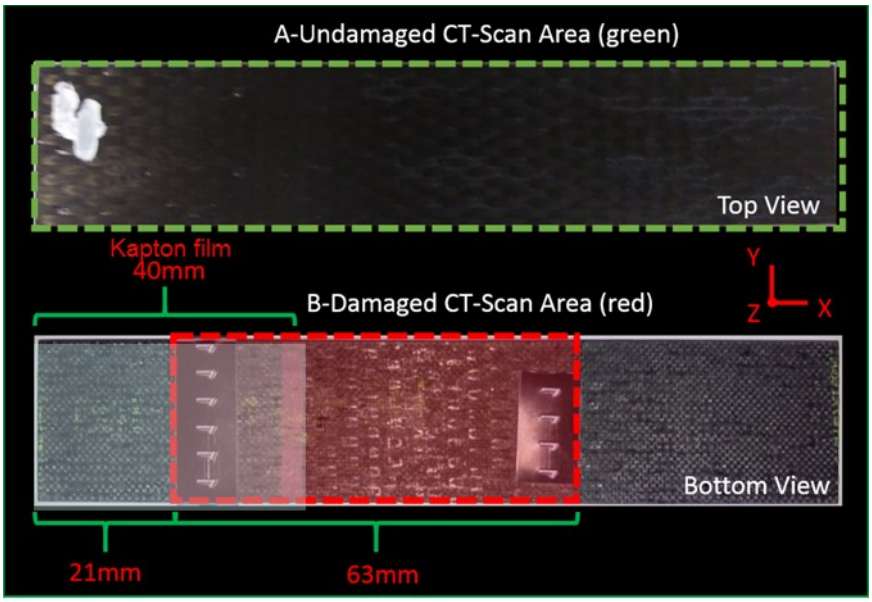

Figure 6: CT-Scan Scan Areas

Assessment of the CT-Scan results was done by taking multiple planes; through the thickness (Z-Axis), along the breadth (Y-Axis) and along the length (X-Axis) of the samples (refer to Figure 7, Figure 8 and Figure 9 below). In the case of the undamaged sample 8 planes were used for each axis with the distances between these planes shown in Figure 7. It should be noted that each plane started on the edge of the relative surface, for example: the X1 plane starts on the edge of the length surface and then shifts 3mm for each further plane.

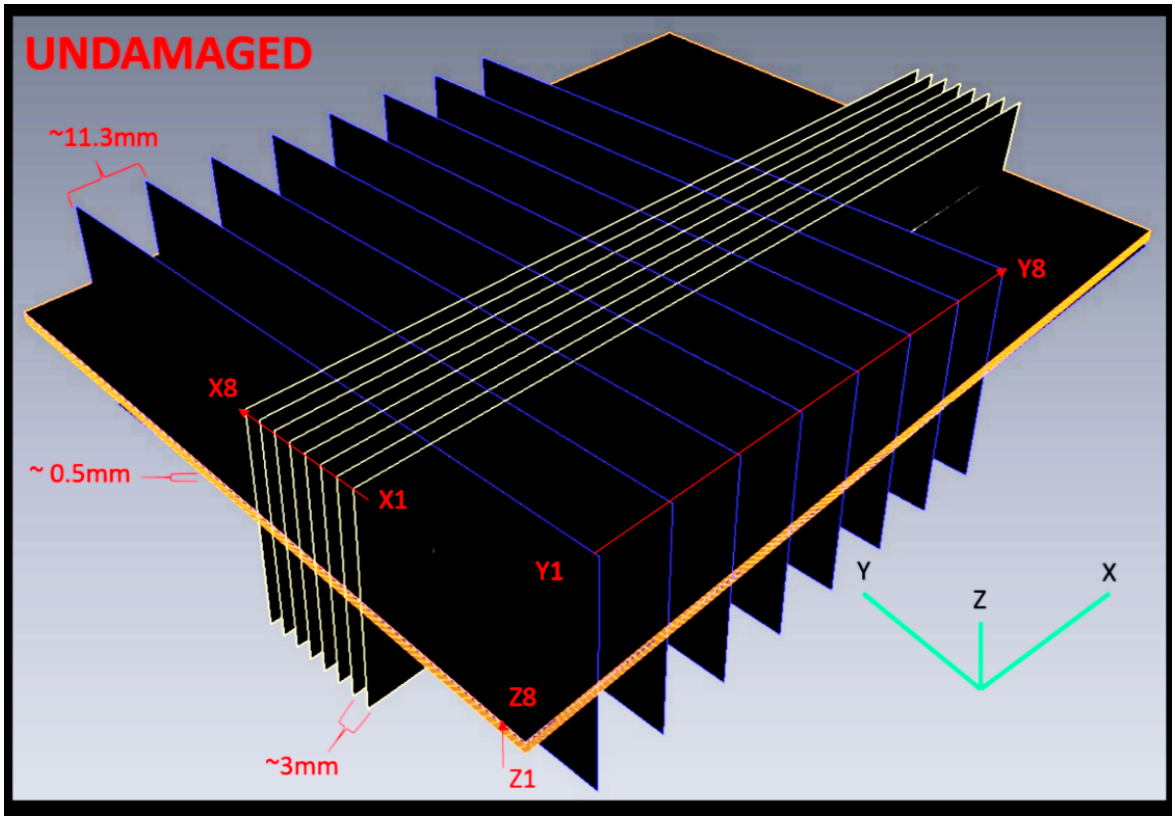

Figure 7: Undamaged CT-Scan Plane Allocation

After damage a smaller area was evaluated near the expected damage regions. A similar plane setup was used, except nine planes were used for the Y-Axis. Y9 was used to evaluate an area were damage was not expected to occur, while planes Y1-Y8 were used to evaluate damage regions.

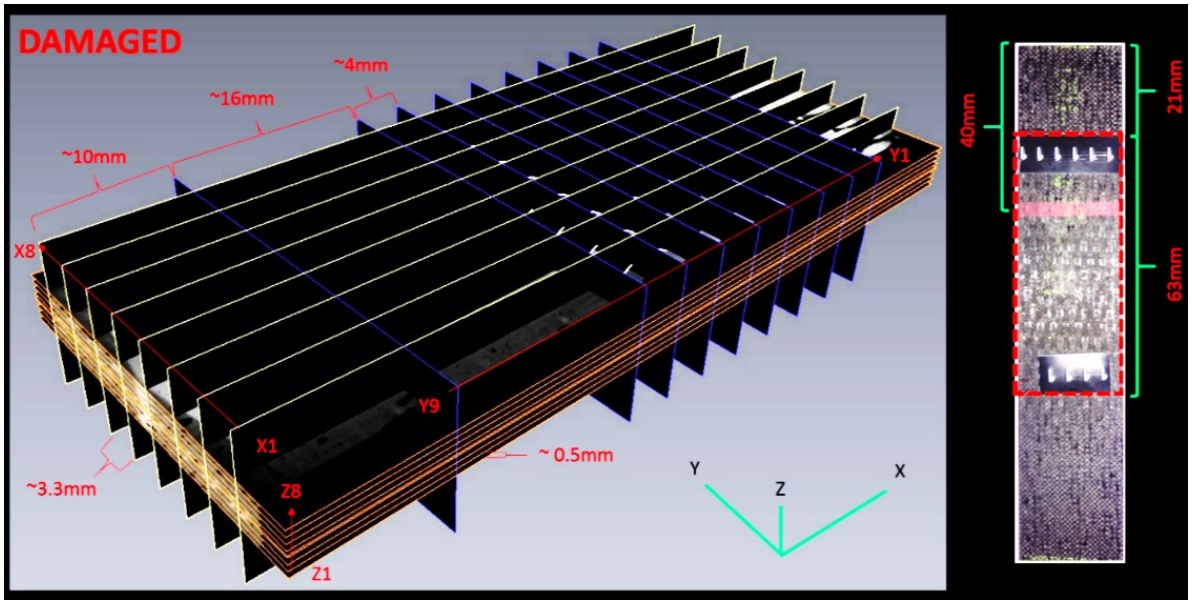

Figure 8: Damaged CT-Scan Plane Allocation

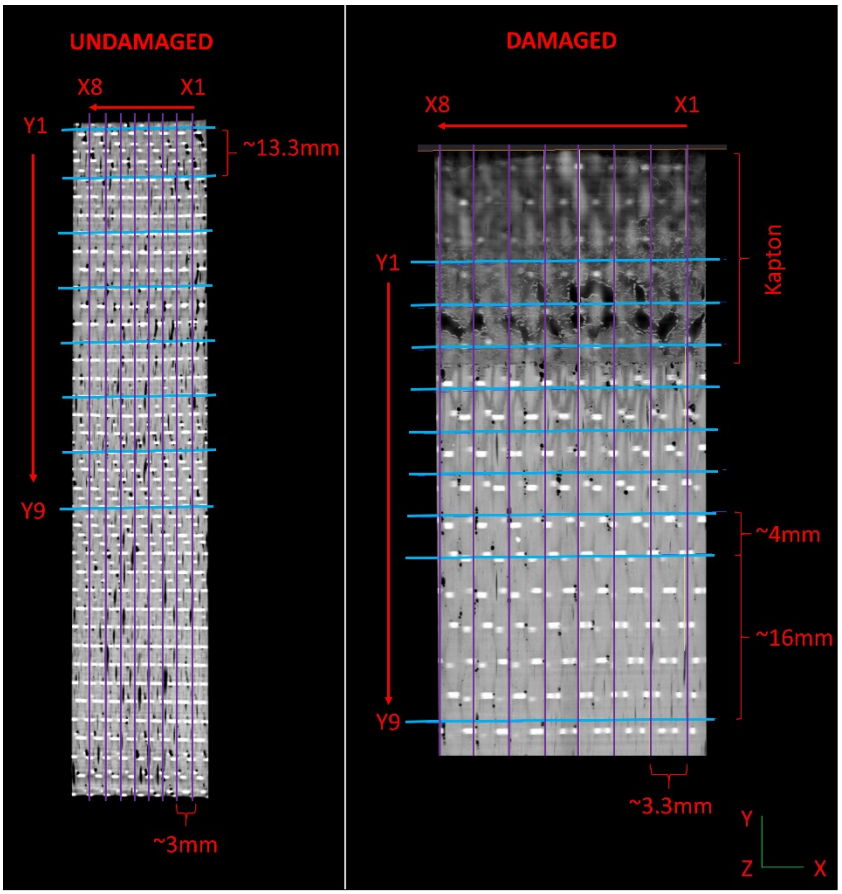

Figure 9: X and Y Axis Plane allocation

5.1.1. CT-Scan Results

Figure 10, Figure 11 and Figure 13 below show the Z, X and Y-Axis planes for S1, respectively. Figure 10 focuses on the damage layer plane and shows the damage through the six damage and healing cycles. Figure 10 (a) shows the damage generated after the first damage cycle vs. an undamaged area, the areas between the weaved composite fibres becomes darker after the damage is

sustained during the mechanical tests. Due to the orientation and propagation of the damage along the Z-Axis, it becomes difficult to visualise the damage, as one plane cannot sufficiently follow the non-uniform nature of the crack propagation (refer to Figure 11, Figure 13 and Figure 14).

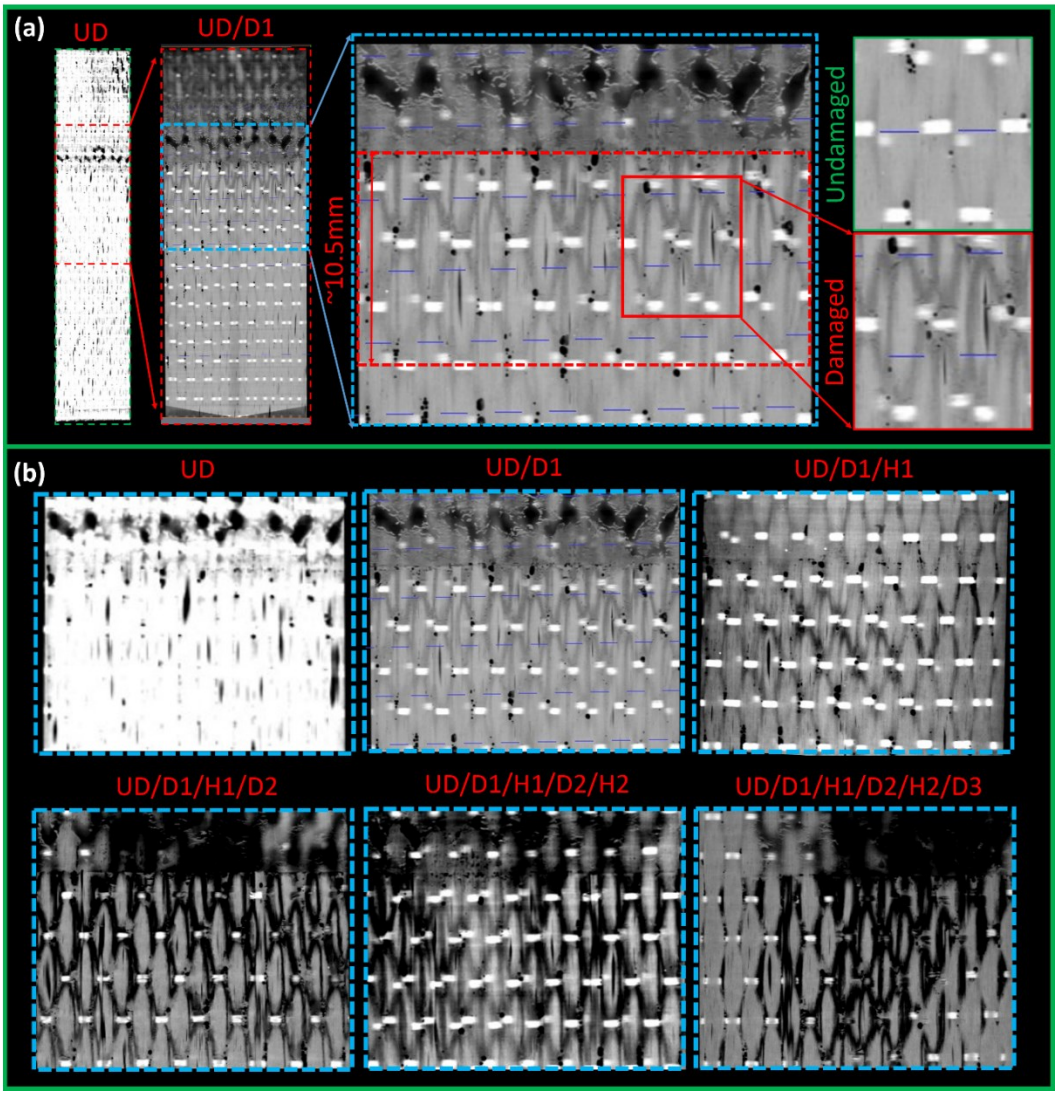

Figure 10: Z-Axis Plane Results for S1 (Damage Layer)

Figure 11 below shows the edge slice (X8), after the first mechanical test, there is clear evidence of an extension in the Kapton layer between UD and D1 (crack propagation – black line extending down from the top middle of the sample). After the first healing cycle (H1) the crack extension has reduced back to the Kapton layer, although this is not clearly visible in the image, through analysis of the Y-Axis Plane (Figure 13) this response was confirmed. While the first damage and healing cycle show healing, the healing between D2 and H2 has reduced. After H2 there is a reduction in the damage region but this reduction is not consistent over the whole length, leaving areas where damage persists (again confirmed during Y-Axis Plane evaluation). The final damage phase shows that damage has grown to the middle of the sample and is clearly evident along the section.

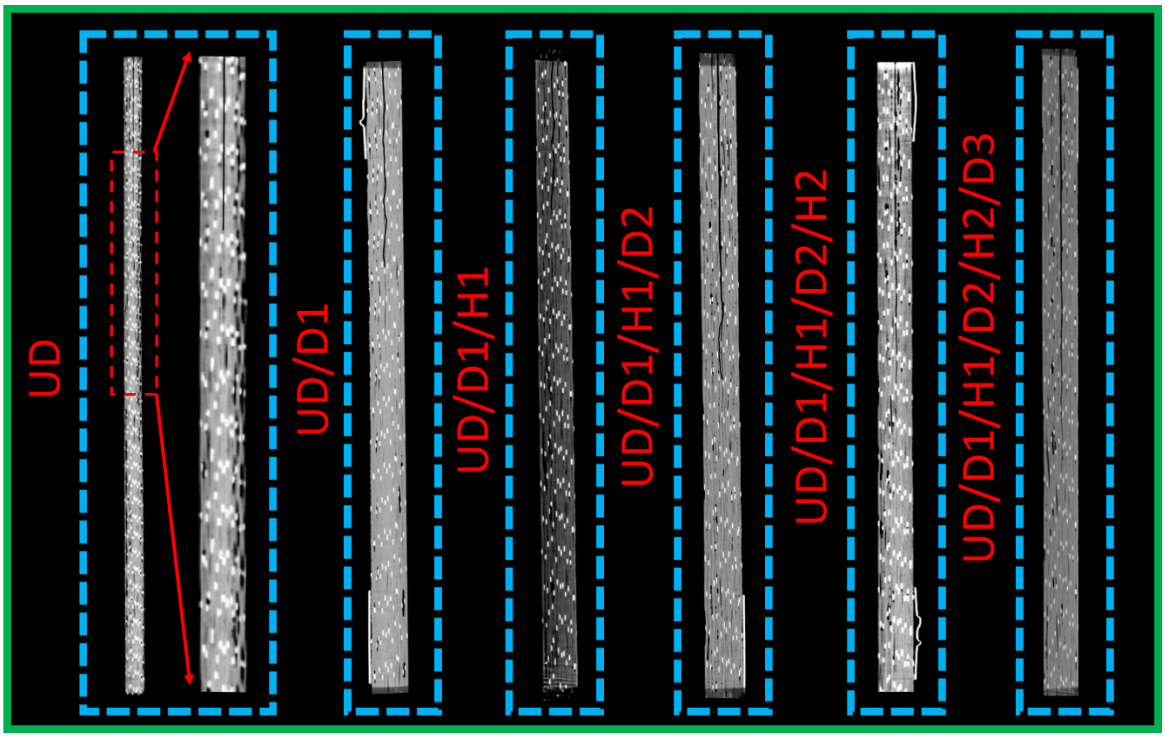

Figure 11: X-Axis Plane Results for S1 (X8)

Using the X-Axis CT-Scan information it is possible to evaluate the extent of damage and recovery for each damage state. Figure 12 below shows the total length of delamination starting from the undamaged state, which includes the 40mm Kapton layer. The diagram clearly shows the recovery of the delamination after each healing cycle, although recovery does occur, the structure weakens after each damage/recovery cycle.

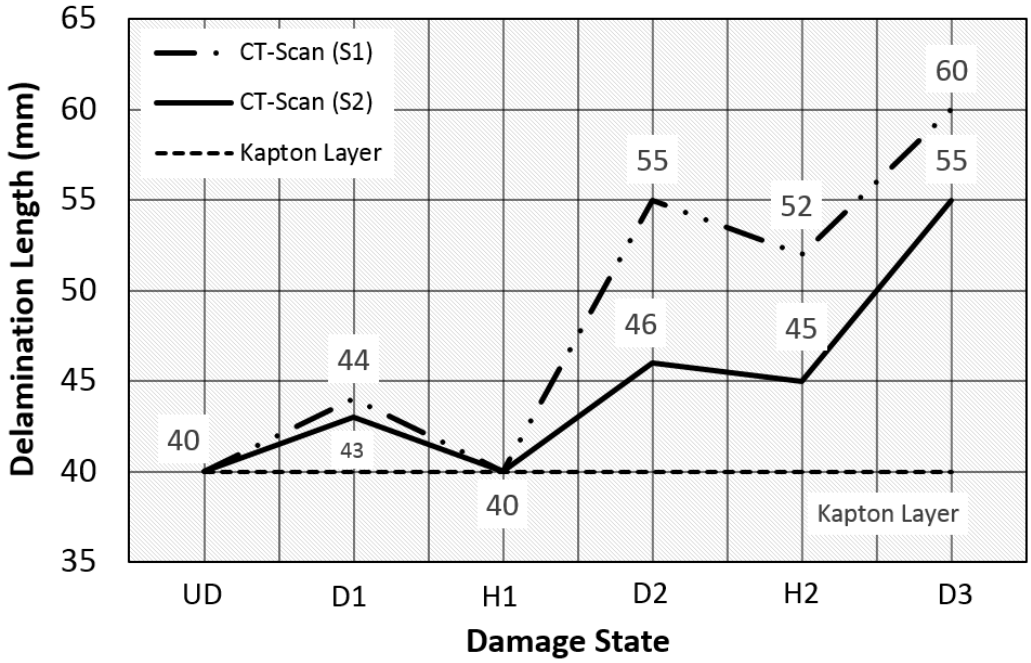

Figure 12: Damage progression and recession for each damage state S1 and S2

While Figure 10 and Figure 11 show the extent of the damage and healing process the results do not clearly show the damage interface with as much detail as the images obtained along the Y plane; which are highlighted in Figure 13 and Figure 14 below. These figures show three points along the

Y-Axis for the last three phases of testing, with Y1 being a cross-section of the Kapton layer, Y5 a cross section of a potential damage region and Y9 being an undamage region (refer to Figure 8). The red uniform line underlines a discontinuity within laminate cross section. A straight line is observed at Y1 section, where kapton layer is laid, while no discontinuity is detected at Y9 section out of the damaged area. In the intermediate location (Y5) a wavy discontinuity underlines a propagating delamination. The material was not able to recover after the second damage/healing cycle (D2/H2), because the crack line is still evident at section Y5 in both the samples.

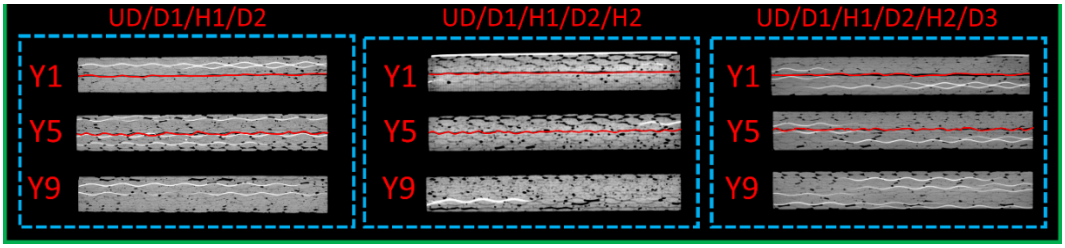

Figure 13: Y-Axis Plane Results for S1

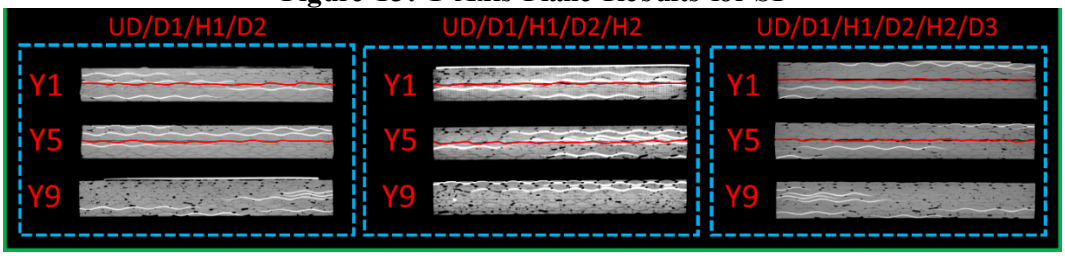

Figure 14: Y-Axis Plane Results for S2

Figure 15 below shows a zoomed image of S2 position Y5 with the delamination visible as the black wavy line through the middle of the sample.

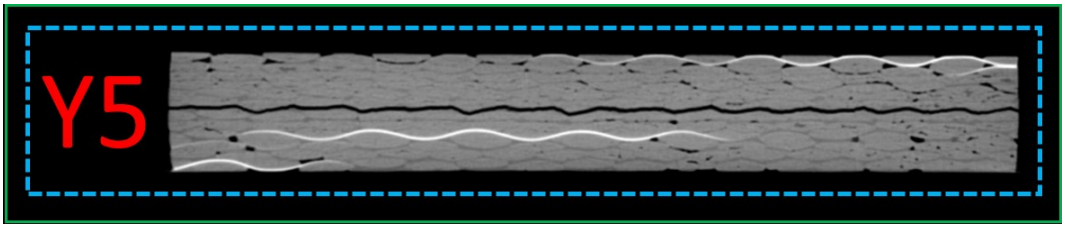

Figure 15: Y-Axis Plane Results for S2, D3 position Y5

5.2. NDT Testing

5.2.1. Standard phased array and water tank C-Scan Results

Standard phased array testing was conducted using a 128 element array at 5MHz. While the water-tank C-Scan was conducted using a single element 35MHz probe (with a step of 0.1mm). These results are shown in Figure 16 and Figure 19 for the two samples tested. Results from the phased array testing show the crack and Kapton layer as white (a large response) while results from the water tank tests are shown as green. From the images, before damage was induced the Kapton layer is visible, with the length being equal to the expected length of 40mm. The crack lengths were calculated as the middle point between the shortest and longest crack point, this was done because the propagation of the crack was not consistent along the width of the sample.
After D1 there is a clear evidence that the crack has propagated from the Kapton area for S1 and S2, in both cases the phased array technique being more accurate and sensitive in detecting the occurred damage. This confirms that damage has in fact occurred after the first damage cycle, this agrees with the mechanical testing. It is evident after H1 that the delaminated area reduces back towards the end of the Kapton layer suggesting healing, although in both cases this does not results in a return to the original undamaged response. Once D2 has been conducted in both S1 and S2 the crack propagation

has exceeded that of the first damage state as the high amplitude responses move further out, this is in line with the CT-Scans that showed a further extension of the crack after D2 (refer to Figure 11). The mechanical testing also showed a weakening of the structure after D2, which would be expected if the structure was not healed back to its undamaged state.

Up until D2 both S1 and S2 behaved in similar manners with respect to the extension of the damage after the damage and healing cycles i.e. the crack extended after damage and receded after healing. After H2, S1 does not appear to heal significantly per the phased array results, small discrepancies are observed in the clamping area The C-scan results show that after H2, the structure seems to be healed up to the cracked layer (which is not consistent with the CT-Scan results, Figure 12), further adding to this inconsistency is the fact that after D3 the delamination does not seem to have propagated further. In Figure 19, S2 shows a clear increase in delamination after D2, reduction after H2 and a further increase after D3 for both the phased array and C-Scan results. It should be noted that on the far right hand side for both samples for D2 and D3 there seems to damage initiation. This was visibly evident during the mechanical testing as splitting between the composite layers at both ends of the sample was observed.

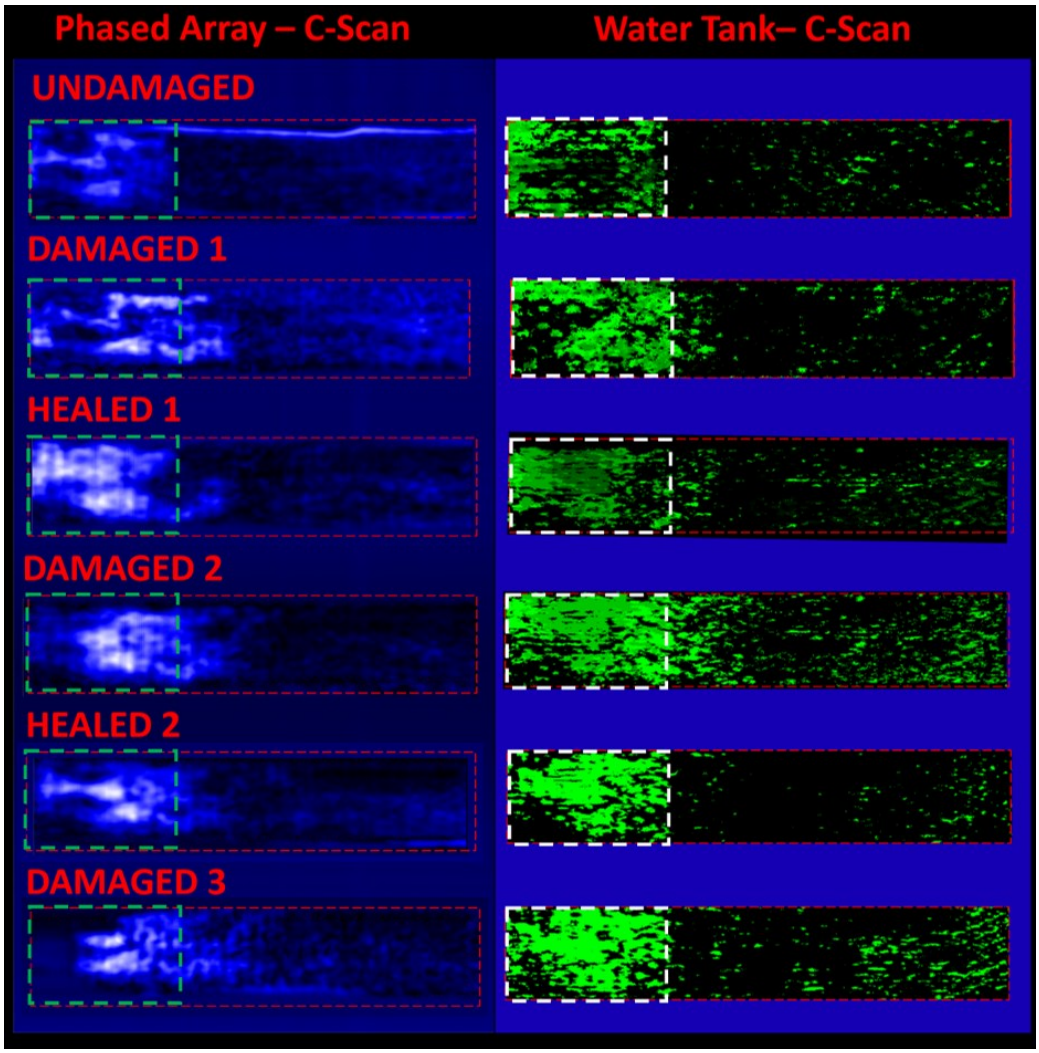

Figure 16: Phased array (5MHz) vs. Water Tank C-Scan (35MHz) S1

Figure 17 shows a comparison of the delamination lengths over the various damage states between the CT-Scan results and the ultrasound testing for S1. S1 was used as the comparison because S2 behaved in a much more consistent manner between the healing and damage cycles. It is evident that the results are consistent for S1 between the CT-Scan and Phased Array testing methods but after D2 for the C-Scan tests it becomes difficult to evaluate the damage extent. Whereas in Figure 18 the different test results show more consistency throughout the whole testing procedure.

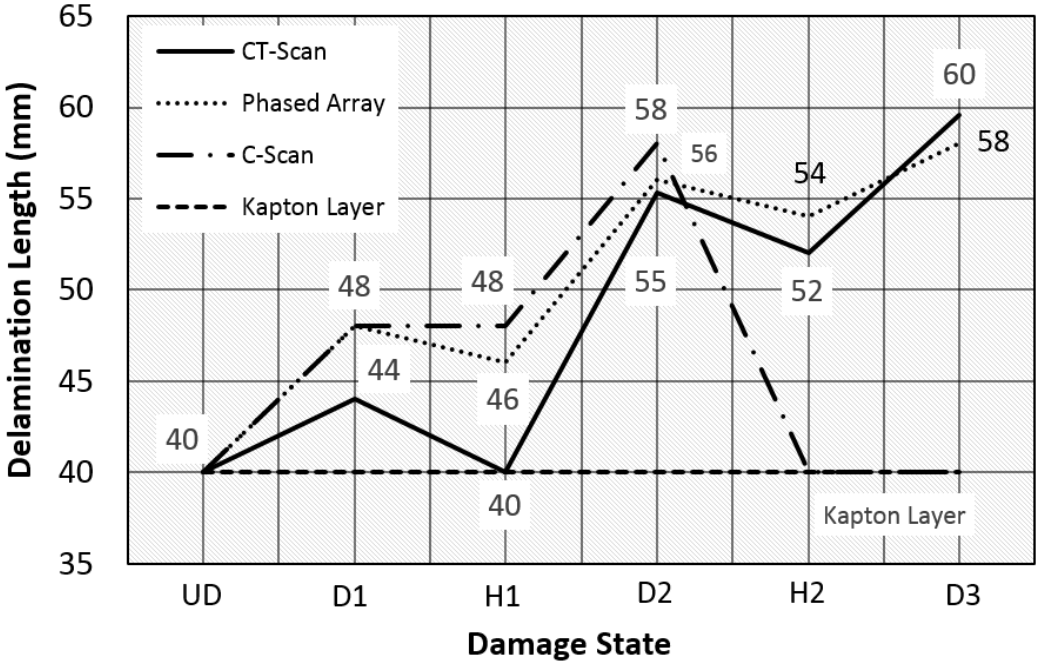

Figure 17: Phased Array and C-Scan results vs. CT-Scan S1

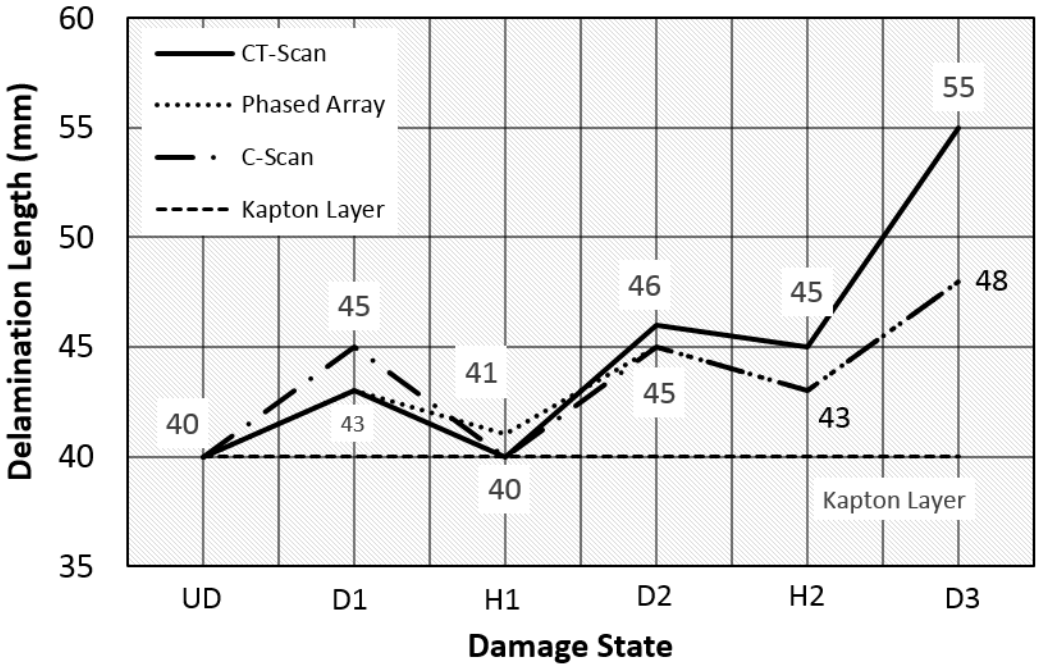

Figure 18: Phased Array and C-Scan results vs. CT-Scan S2

Figure 19 shows the results for S2, unlike S1, there is a clear reduction in the damage area after H2, while D3 clearly shows a further extension of the delamination. The results for S2 are very consistent between the two methods used and show very similar damage propagation and reduction of each successive damage and healing cycle.

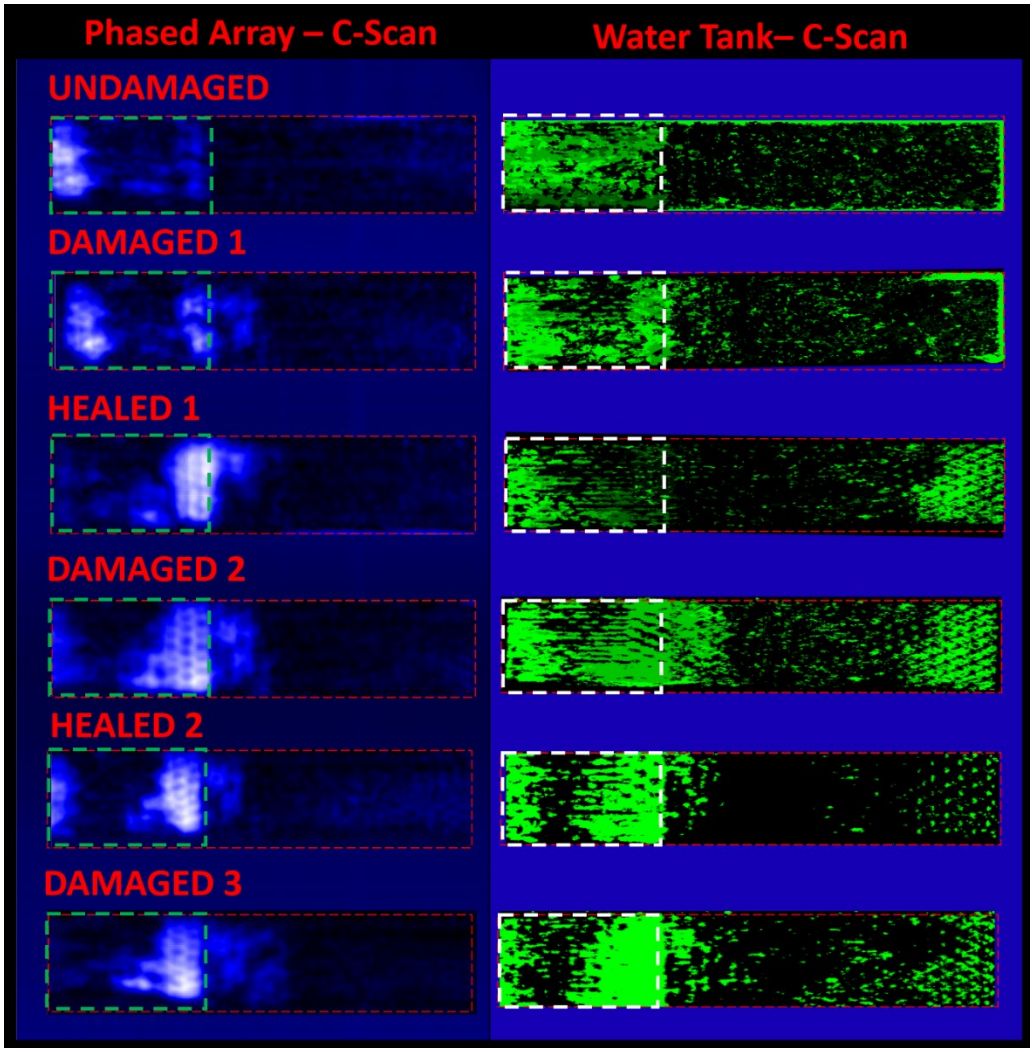

Figure 19: Phased array (5MHz) vs. Water Tank C-Scan (35MHz) S2

5.2.2. Nonlinear Phased array tests

Nonlinear elastic wave spectroscopy (NEWS) techniques are an innovative class of ultrasonic NDE and SHM inspection methods that measure nonlinear elastic effects in the kHz to MHz frequency range to reveal the presence of surface and sub-surface micro-flaws [34-40]. Generally, the interaction of an ultrasonic signal with material is 'linear', with the ultrasonic and material response being linear with respect to the amplitude of the excitation signal. However, linear/conventional ultrasonics are typically only sensitive to large defects and rely on large impedance mismatches caused by open cracks or delaminations, while nonlinear ultrasound relies on the interaction between the ultrasonic signal and discontinuities within the material, in this case related to damage, such as cracks, interfaces and voids. Nonlinear ultrasound relies on these interactions giving rise to higher order harmonics (second, third and fourth harmonics and so forth), sub-harmonics, shifts in the resonance frequencies as well as mixed frequency responses (modulation – two frequency excitation) [41]. The generation of higher order harmonics, which will be used in this piece of work, is attributed to the nonlinearity of the elastic behaviour of the material, with nonlinear Hooke's law at the core of this phenomenon. These techniques have shown higher sensitivity in diagnosing material micro-defects such as porosity, hardening, thermal aging and corrosion when compared to linear ultrasound methods. For this work the second and third order nonlinearity parameters have been simplified in order to determine the nonlinear interaction of imbedded defects. The second (β) and third (γ) order nonlinearity parameter can be described by the equations below [37, 42]:

$$\beta = \frac{8A_2}{A_1^2 k^2 a_1} \propto \frac{A_2}{A_1} \quad (1)$$

$$\gamma \approx \frac{A_3}{A_1}\frac{48}{k^3 a_1} \propto \frac{A_3}{A_1} \quad (2)$$

where: A_1, A_2 and A_3 are the respective frequency amplitudes of the first, second and third harmonics of the recorded time domain waveforms, k is the wavenumber, and a_1 is the propagation distance.

Considering an array with transmitting elements j and receiving element k (Figure 20) the time domain signal with a certain frequency (f) can be represented as $f_{j,k}(t)$, thus the frequency spectrum of a given time window can be expressed as:

$$F(f) = FFT(f_{j,k}(t)) \quad (3)$$

where: f represents the fundamental, second and third harmonic response of the system.

If an ultrasound array is considered and set up as in Figure 20 (a) and (b) below, multiple k transmit and receive positions (pulse-echo testing) will result in multiple time domain response signals for each point tested. The system comprised of a 128 element 5MHz probe half-stepped linear C-Scan of the damage area using a set of 16 elements.

Figure 20: Isometric (a) and cross section (b) view of scan points for an array setup

After considering the frequency spectrum of each captured element it is possible to determine the responses of the higher order harmonics. The simplified nonlinearity parameters were also evaluated (Equation 1 and 2), these results are show in Figure 21 to Figure 25 for S1. Figure 21 shows the fundamental and second harmonic frequency responses for S1 at 1.6MHz. There is a clear increase in the amplitude of responses between the undamaged and first damage cycle. The increase in amplitude is a direct response to damage, as damage is induced in the sample the reflection of ultrasonic waves will result in larger amplitude linear response, while damage will generate nonlinear responses determined by the second harmonic. The results show a clear increase in the amplitude after the first damage cycle. Once H1 had been completed there is a reduction in these areas in a manner to that found with the traditional C-Scan methods. D2 shows a further extension in the

damage region and H2 a slight reduction that is mainly within the Kapton layer, again in line with mechanical results, CT-Scans and C-Scans. D3 provides an even further extension of the damage region, it should be noted that this region extends much further when evaluated using the higher order harmonics and nonlinear parameters than when being evaluated with the fundamental frequency.

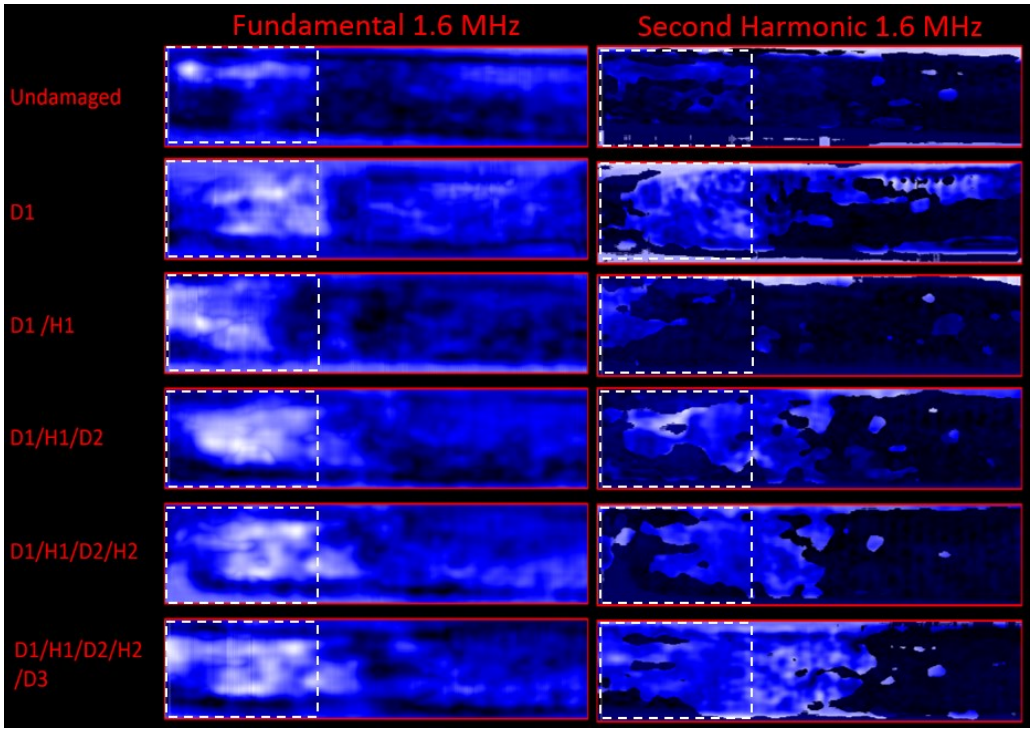

Figure 21: Fundamental frequency response (A_1) Second harmonic response (A_2) S1

Figure 22 and Figure 23 show a comparison between the standard ultrasound results and the fundamental (frequency domain) and nonlinear results. The nonlinear results have been grouped together as they are consistent for all the parameters tested (A_2, A_3, β and γ). The results for the fundamental and nonlinear tests show an improved evaluation of damage at H2 and D3. Although the damage state of S1 does not change between D2 and D3 for the fundamental results. While the nonlinear results suggest no healing has occurred to the right of the Kapton layer between D2 and H2. Healing is observed within the Kapton layer area after H2, as in Figure 16 earlier. The results for S2 are more consistent between the various testing methods, except for the response of the Fundamental, which suggests that very little healing has occurred at H1.

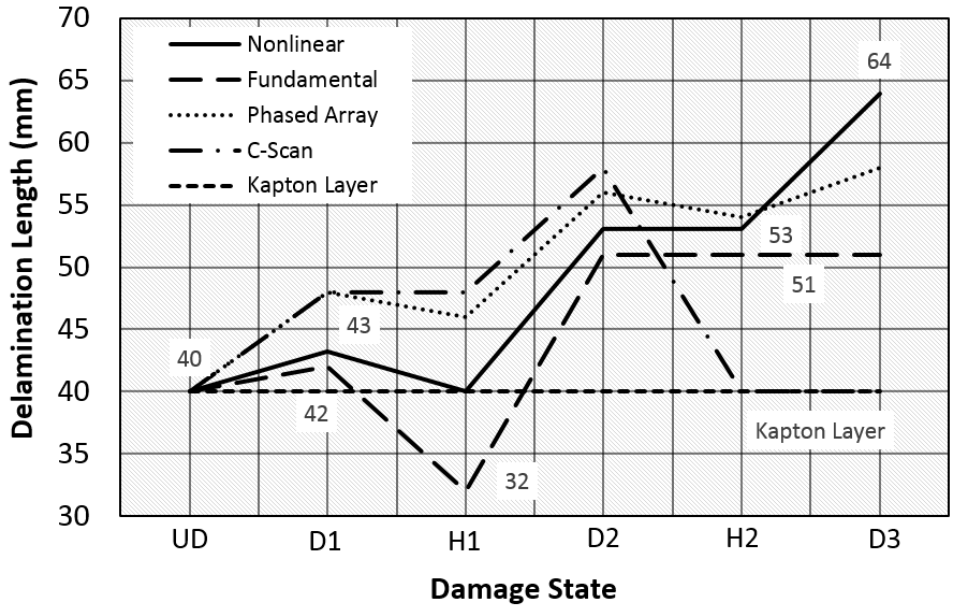

Figure 22: Nonlinear results vs. various ultrasound testing techniques S1

While Figure 21, Figure 22 and Figure 26 indicate that there is healing within the Kapton region according to the fundamental frequency response, this is not the case when re viewing the CT-Scan results nor would this be reasonable to assume considering the presence of the Kapton layer. The fundamental frequency response is calculated as the amplitude determined from the FFT of the time signal through the thickness of the sample. The indicated healing up to 32mm suggests that the amplitude reflection from 32mm to the end of the Kapton layer (40mm) is low relative to the area preceding 32mm (the evident damage area). A reason for this apparent healing can be given by a shift of the Kapton film after the healing process as a result of a non-uniform pressure distribution during the heating process. Thus, the layer does not lie perpendicular to the array, resulting in lower reflections from the Kapton layer to the array or, if at an angle great enough, no reflection at all, resulting in the low amplitude response visualised in Figure 21 (D1/H1).

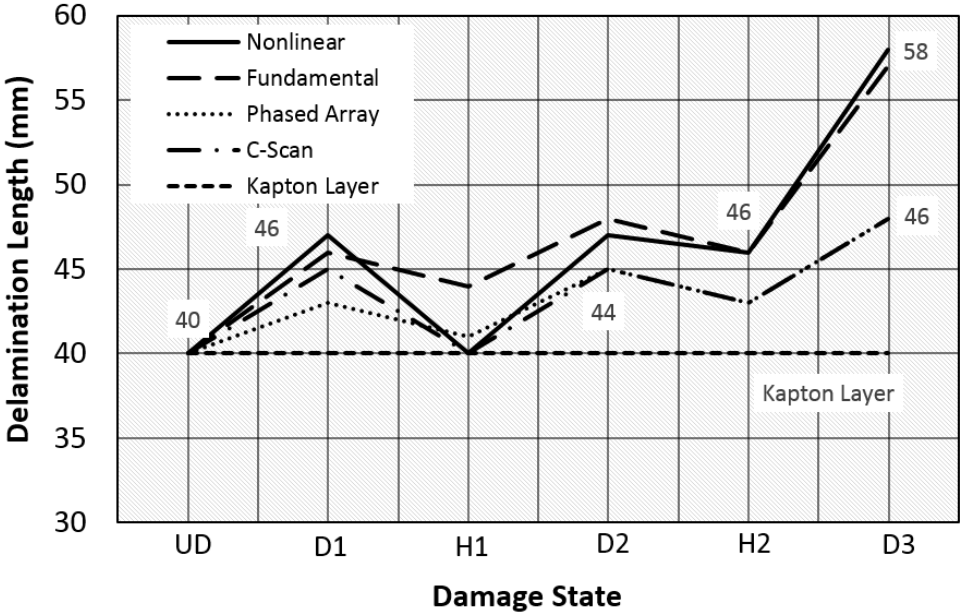

Figure 23: Nonlinear results vs. various ultrasound testing techniques S2

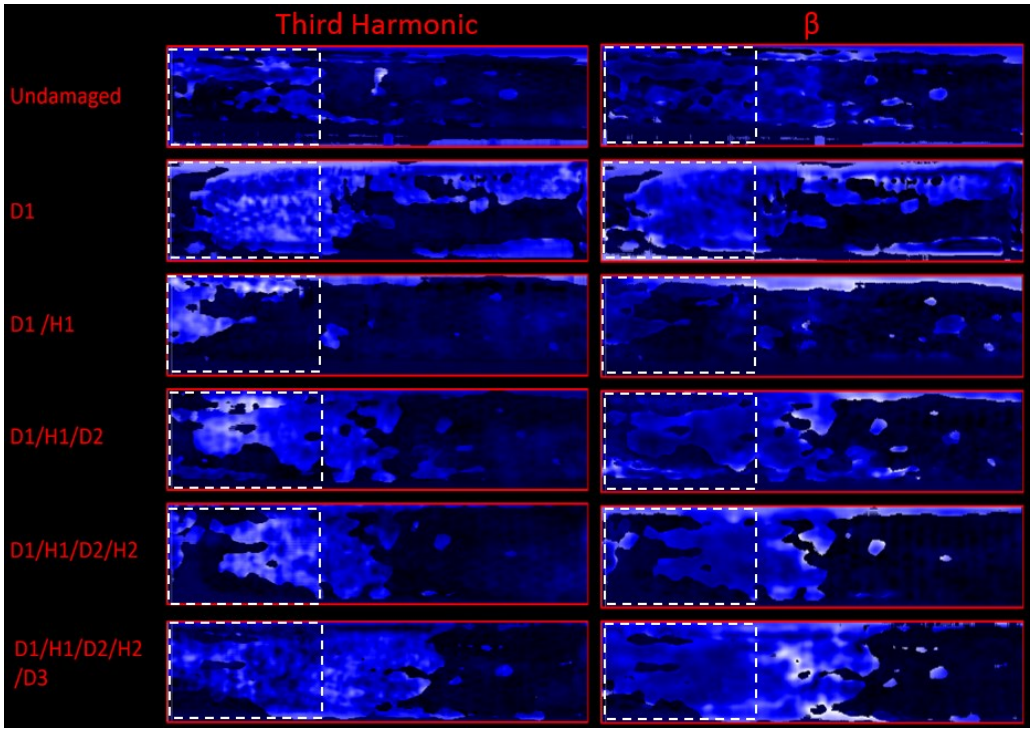

Figure 24: Third harmonic response (A_3) Beta response (β) S1

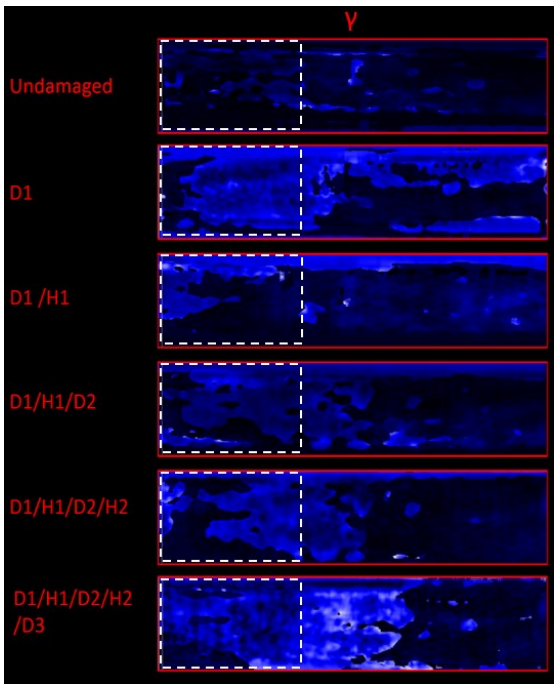

Figure 25: Gamma Response (γ) S1

Figure 26 below compares the fundamental and nonlinear results to those determined by the CT-Scan for S1. The nonlinear results follow the CT-Scan results very closely, and therefore provide good information about the damage state of the sample throughout the investigated process. Surprisingly the fundamental results do not change significantly after the second damage state, suggesting that no healing or further damage was introduced into the sample. The fundamental results although better than those achieved using the traditional methods, would still provide incorrect information regarding the damage state of the structure between D2 and D3. While the nonlinear

method suggests that at H2 there was no reduction in the delamination from the right-hand side of the sample, the images clearly show a reduction in damage within the Kapton area.

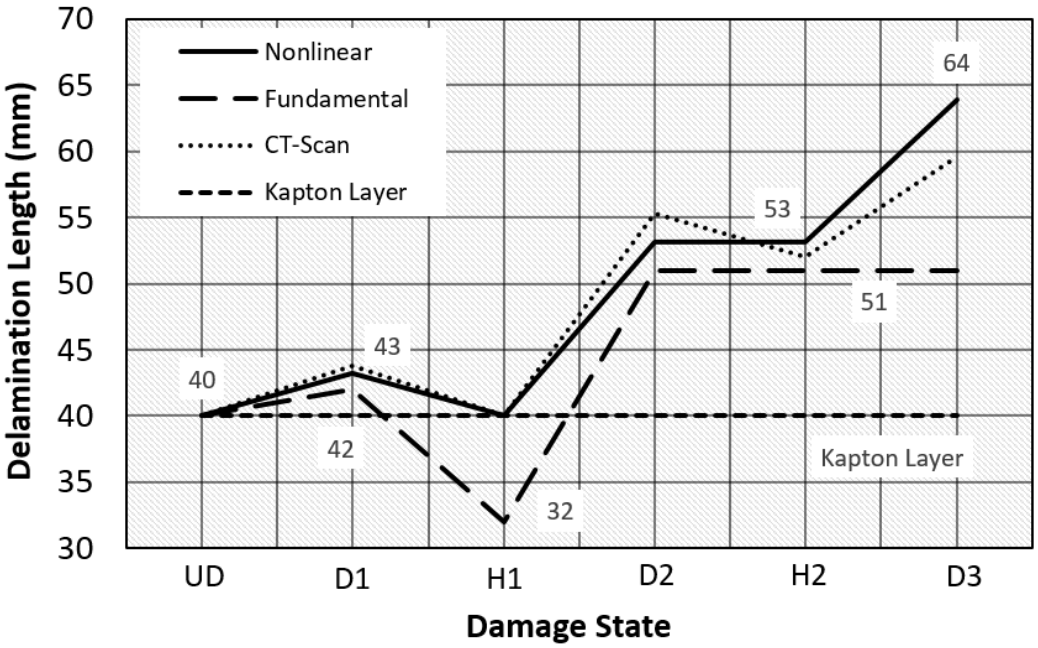

Figure 26: Nonlinear and Fundamental responses vs. CT-Scan Results S1

Multiple ultrasound techniques were evaluated in order to generate a clear understanding of the effectiveness of each detection method to evaluate healing. From a theoretical perspective the water tank C-Scan should be the least effective method due to the fact that it only uses a single element (single transducer) while the phased array consisted of a 128 element transducer with 16 elements used for beam forming. The improved accuracy in the phased array C-Scan is due to beam forming which focuses multiple signals through the thickness of a sample, increasing the excitation energy focused at damage regions, which increases the amplitude of the echo. Linear techniques including the water tank and phased array system rely on impedance mismatches (i.e. changes in densities at interfaces – cracks), which makes the detection of 'closed' cracks (small to no impedance mismatch) difficult using these techniques. Crack propagation during shear testing is likely to generate areas where closed cracks exist, making it difficult for linear techniques to evaluate these regions. Nonlinear methods do not rely on impedance mismatches, but rather excitation (clapping/rubbing) of damage interfaces which result in the generation of further harmonics (second/third etc.). Thus nonlinear methods should be more sensitive to this type of damage and, as it is shown in the results, they more accurately represent the fracture toughness (which will be discussing in the following section) when compared to the CT-Scan (acting as the baseline) than the linear results

6. Characterisation of healing performance

In order to test the effectiveness of the different NDT techniques illustrated in the previous paragraphs, the values of the initial crack length evaluated with both the linear and non-linear phased array for the three different healing/damage cycles were used to calculate the mode II fracture toughness (G_{II}) and the results were compared with the results obtained from the CT-Scan images. Analysing the loading curves obtained during the ENF test, it is possible to observe that the first portion is linear and it corresponds to the initial elastic response of the sample. Once a critical Load (P_{NL}) is reached, the samples show a more complex non-linear behaviour. This change in the response of the sample is due to the ENF sample geometry. Indeed, because of the ductility of the resin and

due to the presence of the initial edge crack, the samples respond to a bending load by showing crack growth and propagation prior to fast fracture. Table 3 illustrates the values of the critical load at the onset of stable crack propagation that were identified for all the curves and the extent of the initial delamination according to the CT-Scan, the linear phased array (LPA) and the non-linear phased array (NLPA).

Table 3: Critical Load values for each damage cycle and extension of the initial crack evaluated by linear and non-linear phased array and compared with CT-Scan measurement

	S1 D1	S1 D2	S1 D3	S2 D1	S2 D2	S2 D3
P_{NL} [N]	780	179	252	650	583	341
initial crack length (a LPA) [mm]	30	36	44	30	31	33
initial crack length (a NLPA) [mm]	30	33	43	30	30	36
initial crack length (a CT Scan) [mm]	30	30	42	30	30	35

From these data it is possible to evaluate the mode II fracture toughness by following the compliance method demonstrated by Cairns et al [43] and using the equation:

$$G_{II} = \frac{9P^2 Ca^2}{2w(2L^3+3a^3)} \quad (4)$$

Where P represents the load at the onset of the delamination propagation, C is the compliance of a simple supported beam with a crack extending from one ledge towards the middle section, a is the length of the initial crack, w is the width of the sample and L the span length used during the test.

The value of the compliance can be calculated from the following equation:

$$C = \frac{2L^3+3a^3}{8Ewh^3} \quad (5)$$

where E represents the elastic modulus of the material and h is half of the thickness of the sample.

The values of the fracture toughness calculated for both samples over the three healing/damage cycles with linear and non-linear phased array and CT-Scan are represented in Figure 27 and Figure 28.

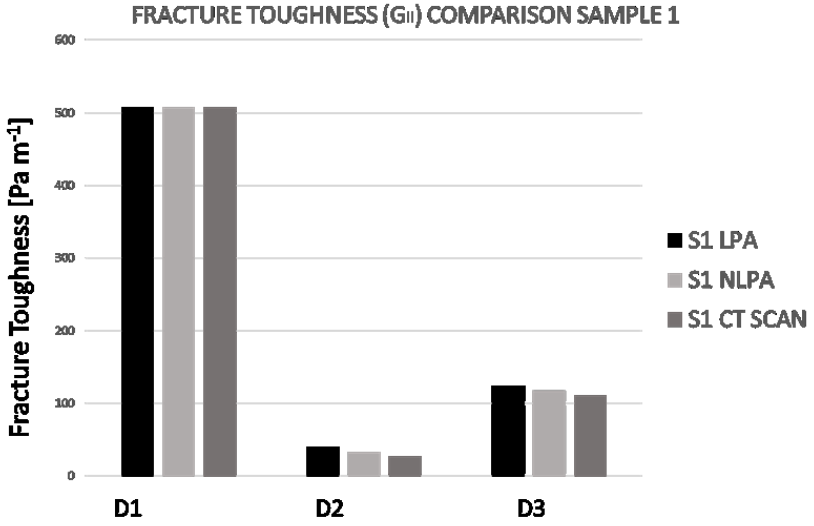

Figure 27: Comparison between fracture toughness of S1 evaluated from linear and non-linear phased array inspection and compared with CT-Scan analysis data.

As it is possible to see from Figure 27, in case of S1 after the first damage cycle (which has the same value because the initial crack length was given by the Kapton layer) the values of GII are strongly affected by the different techniques used. It is important to remember that the CT-Scan results of the crack length, in this case, are being used as the baseline as the CT-Scan is the most accurate method available. By determining the fracture toughness (directly related to the crack length) of the linear and NLPA methods and comparing them to the CT-Scan results, it is possible to measure which method more accurately determines the damage state of the sample. Therefore, the calculated percent error between the fracture toughness of the linear and NLPA against the CT-Scan provides a quantitative method to determine which technique is more accurate. The error between the linear phased array and the CT-Scan was +48.1% (vs +22.5% of the NLPA) for the second cycle and +11.4% (vs +5.5% of the NLPA) for the third cycle, which showed an error of twice that determined using the NLPA. Therefore it is clear that the non-linear phased array technique is more accurate than the linear technique as it more accurately describes the damage state of the sample. Furthermore it is important to underline that the NLPA is also more accurate in the case of the incomplete or partial healing (D2).

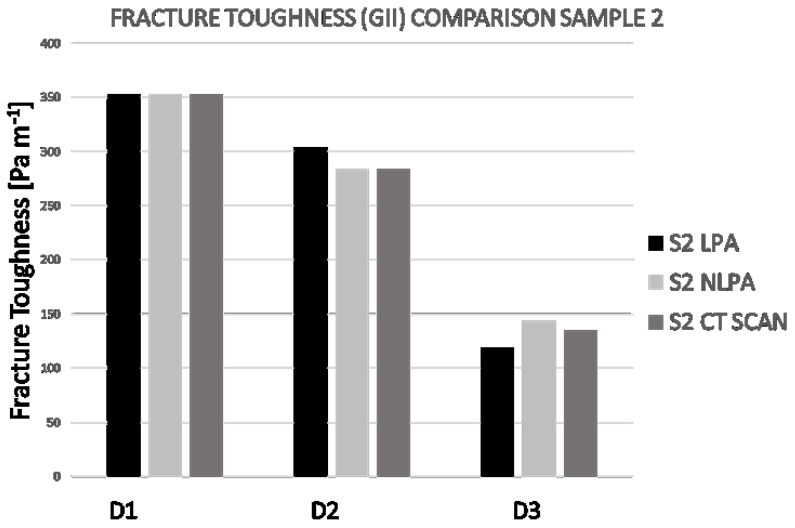

Figure 28: Comparison between fracture toughness of S2 evaluated from linear and non-linear phased array inspection and compared with CT-Scan analysis data.

Results from S2 are illustrated in Figure 28 and they are consistent with what observed in the previous sample. Indeed, also in this case it is possible to clearly see that the increased accuracy of the non-linear analysis reduces the error with the CT-Scan. In particular, during the second healing/damage cycle (D2) it is possible to observe that while the LPA technique gives an error of +7.2%, the NLPA method shows exactly the same reading of the CT-Scan measurement. As for the third cycle, results in D3 show an error of the LPA of -11.97%, while NLPA data decreases this difference to +6.65%. The samples studied showed a quite different sensibility to the healing treatment. The S1 sample recovered its mode II strength with lower efficiency compared to the S2 sample. Even if the neat resin proved its capability to recover severe damages after thermally activated healing, selection of effective healing procedures and parameters are quite critical and are beyond the context of the present paper.

7. Conclusions

The performance of different non-destructive techniques in assessing the effectiveness of thermally activated self-healing polymers based on reversible Diels–Alder reaction was investigated during multiple damage/healing cycles.
Five successive damaged and healed states were studied using nonlinear ultrasound techniques by measuring the extent of damage propagation and healing recovery during each cycle. The results

were compared to standard linear ultrasound and benchmarked against CT-Scan results. While linear phased array techniques provide a good approximation of the extent and recover of damage in the structure, in some cases they fail to provide a clear and accurate image of damage evolution. The increased accuracy of the non-linear approach to detect bonded regions over the traditional linear phased array was shown by evaluating the values of mode II fracture toughness. Results from the experimental campaign showed that in the passage from a linear to a nonlinear approach, it is possible to increase the resolution of the analysis, reducing the difference with the CT-Scan readings up to 50%. This work demonstrated the successful use of a nonlinear ultrasound phased array method for the assessment of the efficiency of recovery of self-healing samples.

Acknowledgements

The activities were performed in the frame of the project "A Life-cycle Autonomous Modular System for Aircraft Material State Evaluation and Restoring System – ALAMSA, FP7 Grant Agreement 314768"

References:

[1] S. W. Tsai, "Structural Behavior of Composite Materials," DTIC Document (1964).
[2] W. Cantwell and J. Morton, "The impact resistance of composite materials—a review," *composites* 22(5), 347-362 (1991)
[3] T. Mauldin and M. Kessler, "Self-healing polymers and composites," *International Materials Reviews* (2013)
[4] B. Blaiszik, S. Kramer, S. Olugebefola, J. S. Moore, N. R. Sottos and S. R. White, "Self-healing polymers and composites," *Annual Review of Materials Research* 40(179-211 (2010)
[5] P. Zhang and G. Li, "Advances in healing-on-demand polymers and polymer composites," *Progress in Polymer Science* 57(32-63 (2016)
[6] Y.-L. Liu and T.-W. Chuo, "Self-healing polymers based on thermally reversible Diels–Alder chemistry," *Polymer Chemistry* 4(7), 2194-2205 (2013)
[7] S. Dello Iacono, A. Martone, G. Filippone, D. Acierno, M. Zarrelli, M. Giordano and E. Amendola, "Insight on mendable resin made by combining Diels-Alder epoxy adducts with DGEBA," in *VIII INTERNATIONAL CONFERENCE ON "TIMES OF POLYMERS AND COMPOSITES": From Aerospace to Nanotechnology*, p. 020075, AIP Publishing (2016).
[8] J. Canadell, H. Goossens and B. Klumperman, "Self-healing materials based on disulfide links," *Macromolecules* 44(8), 2536-2541 (2011)
[9] H. Zhang, H. Xia and Y. Zhao, "Poly (vinyl alcohol) hydrogel can autonomously self-heal," *Acs Macro Letters* 1(11), 1233-1236 (2012)
[10] D. Y. Wu, S. Meure and D. Solomon, "Self-healing polymeric materials: a review of recent developments," *Progress in Polymer Science* 33(5), 479-522 (2008)
[11] S. R. White, N. R. Sottos, P. H. Geubelle, J. S. Moore, M. R. Kessler, S. R. Sriram, E. N. Brown and S. Viswanathan, "Autonomic healing of polymer composites," *Nature* 409(6822), 794-797 (2001)
[12] M. Samadzadeh, S. H. Boura, M. Peikari, S. Kasiriha and A. Ashrafi, "A review on self-healing coatings based on micro/nanocapsules," *Progress in Organic Coatings* 68(3), 159-164 (2010)

[13] I. P. Bond, R. S. Trask, H. R. Williams and G. J. Williams, "Self healing fibre-reinforced polymer composites: an overview," in *Self Healing Materials*, pp. 115-138, Springer (2007).
[14] K. S. Toohey, N. R. Sottos, J. A. Lewis, J. S. Moore and S. R. White, "Self-healing materials with microvascular networks," *Nat Mater* 6(8), 581-585 (2007)
[15] E. L. Kirkby, J. D. Rule, V. J. Michaud, N. R. Sottos, S. R. White and J. A. E. Månson, "Embedded Shape-Memory Alloy Wires for Improved Performance of Self-Healing Polymers," *Advanced Functional Materials* 18(15), 2253-2260 (2008)
[16] G. Li, H. Meng and J. Hu, "Healable thermoset polymer composite embedded with stimuli-responsive fibres," *Journal of The Royal Society Interface* rsif20120409 (2012)
[17] E. D. Rodriguez, X. Luo and P. T. Mather, "Linear/network poly (ε-caprolactone) blends exhibiting shape memory assisted self-healing (SMASH)," *ACS applied materials & interfaces* 3(2), 152-161 (2011)
[18] D. Homma, H. Mihashi and T. Nishiwaki, "Self-healing capability of fibre reinforced cementitious composites," *Journal of Advanced Concrete Technology* 7(2), 217-228 (2009)
[19] L. Zedler, M. D. Hager, U. S. Schubert, M. J. Harrington, M. Schmitt, J. Popp and B. Dietzek, "Monitoring the chemistry of self-healing by vibrational spectroscopy–current state and perspectives," *Materials Today* 17(2), 57-69 (2014)
[20] C.-W. In, R. B. Holland, J.-Y. Kim, K. E. Kurtis, L. F. Kahn and L. J. Jacobs, "Monitoring and evaluation of self-healing in concrete using diffuse ultrasound," *NDT & E International* 57(36-44 (2013)
[21] W. Zhong and W. Yao, "Influence of damage degree on self-healing of concrete," *Construction and Building Materials* 22(6), 1137-1142 (2008)
[22] A. M. Coppola, P. R. Thakre, N. R. Sottos and S. R. White, "Tensile properties and damage evolution in vascular 3D woven glass/epoxy composites," *Composites Part A: Applied Science and Manufacturing* 59(9-17 (2014)
[23] S. Granger, G. P. Cabot, A. Loukili, D. Marlot and J. Lenain, "Monitoring of cracking and healing in an ultra high performance cementitious material using the time reversal technique," *Cement and Concrete Research* 39(4), 296-302 (2009)
[24] E. Amendola, S. D. Iacono, A. Pastore, M. Curcio, M. Giordano and A. Iadonisi, "Epoxy thermosets with self-healing ability," *J. Mater. Sci. Chem. Eng* 3(7), 162-167 (2015)
[25] W. Tang, O. Kardani and H. Cui, "Robust evaluation of self-healing efficiency in cementitious materials–a review," *Construction and Building Materials* 81(233-247 (2015)
[26] G. Li and M. John, "A self-healing smart syntactic foam under multiple impacts," *Composites Science and Technology* 68(15), 3337-3343 (2008)
[27] M. John and G. Li, "Self-healing of sandwich structures with a grid stiffened shape memory polymer syntactic foam core," *Smart Materials and Structures* 19(7), 075013 (2010)
[28] Ö. Oralkan, A. S. Ergun, J. A. Johnson, M. Karaman, U. Demirci, K. Kaviani, T. H. Lee and B. T. Khuri-Yakub, "Capacitive micromachined ultrasonic transducers: Next-generation arrays for acoustic imaging?," *Ultrasonics, Ferroelectrics, and Frequency Control, IEEE Transactions on* 49(11), 1596-1610 (2002)
[29] R. Y. Chiao and L. J. Thomas, "Analytic evaluation of sampled aperture ultrasonic imaging techniques for NDE," *Ultrasonics, Ferroelectrics, and Frequency Control, IEEE Transactions on* 41(4), 484-493 (1994)

[30] A. Sugawara, K. Jinno, Y. Ohara and K. Yamanaka, "Closed-crack imaging and scattering behavior analysis using confocal subharmonic phased array," *Japanese Journal of Applied Physics* 54(7S1), 07HC08 (2015)
[31] Y. Ohara, T. Mihara, R. Sasaki, T. Ogata, S. Yamamoto, Y. Kishimoto and K. Yamanaka, "Imaging of closed cracks using nonlinear response of elastic waves at subharmonic frequency," *Applied physics letters* 90(1), 011902 (2007)
[32] J. Potter, A. Croxford and P. Wilcox, "Nonlinear ultrasonic phased array imaging," *Physical review letters* 113(14), 144301 (2014)
[33] C.-S. Park, J.-W. Kim, S. Cho and D.-c. Seo, "A high resolution approach for nonlinear sub-harmonic imaging," *NDT & E International* 79(114-122 (2016)
[34] G. P. M. Fierro and M. Meo, "Nonlinear imaging (NIM) of flaws in a complex composite stiffened panel using a constructive nonlinear array (CNA) technique," *Ultrasonics* 74(30-47 (2017)
[35] F. Ciampa and M. Meo, "Nonlinear elastic imaging using reciprocal time reversal and third order symmetry analysis," *The Journal of the Acoustical Society of America* 131(6), 4316-4323 (2012)
[36] G. M. Fierro, F. Ciampa, D. Ginzburg, E. Onder and M. Meo, "Nonlinear ultrasound modelling and validation of fatigue damage," *Journal of Sound and Vibration* 343(121-130 (2015)
[37] J. H. Cantrell, "Fundamentals and applications of non-linear ultrasonic nondestructive evaluation," *Ultrasonic non-destructive evaluation* vol. 6(Boca Raton (FL): CRC Press), p.363-434 (2004)
[38] G. P. M. Fierro, D. Ginzburg, F. Ciampa and M. Meo, "Nonlinear thermosonics and laser vibrometry for barely visible impact damage of a composite stiffener panel," in *SPIE Smart Structures and Materials+ Nondestructive Evaluation and Health Monitoring*, pp. 980419-980419-980419, International Society for Optics and Photonics (2016).
[39] J. H. Cantrell and W. T. Yost, "Nonlinear ultrasonic characterization of fatigue microstructures," *International Journal of fatigue* 23(487-490 (2001)
[40] S. Boccardi, D. CALLA, G.-P. FIERRO, F. Ciampa and M. Meo, "Nonlinear Damage Detection and Localisation Using a Time Domain Approach," *Structural Health Monitoring 2015* (2015)
[41] G. P. M. Fierro and M. Meo, "Residual fatigue life estimation using a nonlinear ultrasound modulation method," *Smart Materials and Structures* 24(2), 025040 (2015)
[42] M. Meo, F. Amerini and M. Amura, "Baseline-free estimation of residual fatigue life using third order acoustic nonlinear parameter," *The Journal of the Acoustical Society of America* 4(130), 1829-1837 (2010)
[43] D. S. Cairns, "Static and dynamic mode II strain energy release rates in toughened thermosetting composite laminates," *Journal of Composites, Technology and Research* 14(1), 37-42 (1992)